Phase diagram of a model anticlustering binary mixture in two dimensions: A semi-grand-canonical Monte Carlo study

S. Sengupta,* D. Marx,† P. Nielaba, and K. Binder
Institut für Physik, Johannes Gutenberg–Universität Mainz, KoMa 331, D–55099 Mainz, Germany
(Received 30 September 1993)

The temperature-density phase diagram of a model binary mixture in two dimensions is investigated using a semi-grand-canonical Monte Carlo simulation scheme which allows for exchange between the two species while keeping the total number of atoms fixed. The gas-liquid and the gas-solid regions of the phase diagram are mapped out using the efficient block analysis method incorporating finite-size scaling of the various coexisting densities. An ordered *square* lattice structure is seen to be stable at low temperatures. Interesting short-range ordering phenomena resulting in a "disorder line" in the *fluid* phase are also analyzed and compared with results from liquid-state integral equation theories.

PACS number(s): 64.70.Dv, 61.20.Ja, 64.70.−p

I. INTRODUCTION

The study of binary alloys which tend to form ordered structures is an active subject of research because of their theoretical and technological interest. Lattice models of binary alloys [1] have yielded much insight regarding phase stability in these systems. Models consisting of two species of atoms A and B occupying lattice sites and interacting with (antiferromagnetic) Ising-like Hamiltonians have been used to study order-disorder transitions [1] in realistic substitutional alloys such as Cu-Au or Fe-Al. Ordering phenomena in such *lattice* systems are by now rather well studied [1] using a variety of techniques such as, e.g., computer simulations [2,3], mean-field [4], and cluster variational theories [5,6]. On the other hand, whole categories of questions remained untouched and are as yet unanswered. Hardly any theoretical work exists studying these alloys (or simplified models) in their *liquid* phase trying to understand the interplay of the ordering tendencies with packing considerations; most simulations of binary liquids study systems whose constituents are distinguished only through a difference in their atomic sizes [7]. Simple A-B ordering will be frustrated in close-packed structures (e.g., fcc lattices in three and the triangular lattices in two dimensions) and so interesting effects are bound to arise in the liquid phase where the ordering tendency competes with the formation of locally compact structures (dodecahedrons and icosahedrons in three and hexagons in two dimensions) in the high density fluid phase. An immediate question which arises is whether it is at all possible to have a liquid (in addition to the fluid phase) and thus a *liquid*-gas transition in these systems, and whether there is any short-ranged or long-ranged ordering phenomenon possible in the *nonsolid* phases. A related question can be addressed: are there any precursor effects of superstructure ordering in the melt of an ordered alloy?

In this paper we make a first step towards that direction and study the phase diagram of a binary mixture of two constituents A and B such that there are short-ranged attractive interactions between atoms of opposite species and repulsive interactions between those of the same species (in addition to the core-core repulsion). We choose to study our system in two dimensions since it is computationally less demanding and since we are interested in frustration effects which would probably be larger in two rather than in three dimensions. Also, our model may have some experimental relevance in systems of adsorbed molecules on substrates [8] where the interaction is anti-ferromagnetic as opposed to a ferromagnetic case studied previously [9–11].

The central result of this paper, namely, the phase diagram of our prototype model system, is shown in Fig. 1(a). We see that the anticlustering or ordering interaction gives rise to a low-temperature A-B ordered *square*-lattice solid phase [see Fig. 1(c) for a snapshot], which coexists with a gas. At higher temperatures there is a small region where we observe coexisting gas and liquid phases [Fig. 1(b)]. An interesting feature we reveal is that the liquid actually possesses *short-ranged* A-B ordering below a temperature $T_{\rm ord}(\rho)$, which is also shown in Fig. 1(a) as a "disorder line." Understanding the interplay between the standard gas-liquid-solid transitions and the order-disorder phenomena of binary mixtures hence is the general theme of our study.

The organization of the rest of the paper is as follows. We start with introducing our model binary fluid, the simulational details, and the block analysis technique for calculating the phase diagram in Secs. II A, II B, and

*Present address: Material Science Division, Indira Gandhi Center for Atomic Research, Kalpakkam 603 102, Tamil Nadu, India.
†Present address: IBM Research Division, Zurich Research Laboratory, Säumerstr. 4, CH–8803 Rüschlikon, Switzerland.

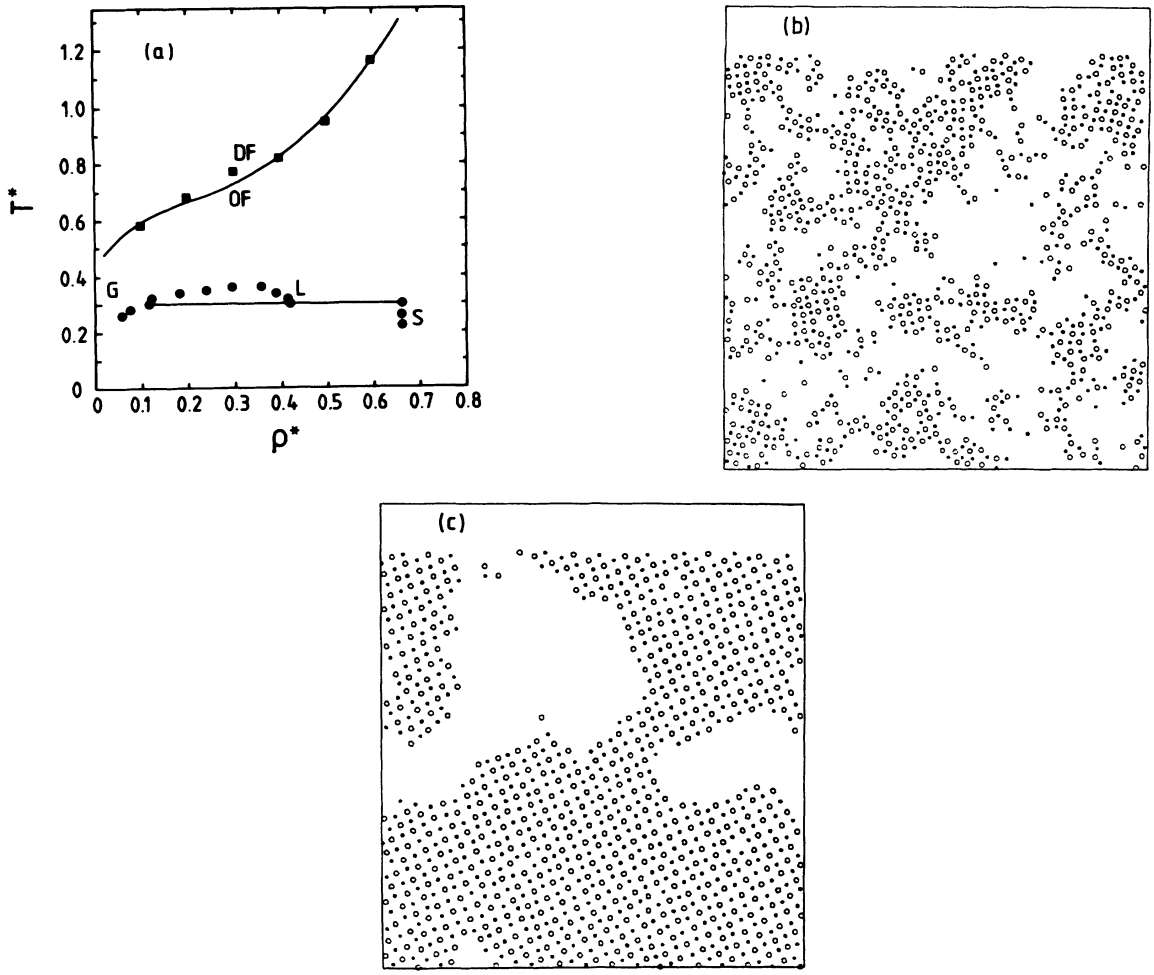

FIG. 1. (a) Temperature-density phase diagram of the anticlustering binary mixture as obtained from Monte Carlo simulations. Circles denote phase coexistence points for the gas (G), liquid (L), and A-B ordered square lattice solid (S) phases; the horizontal line denotes the triple temperature. The "disorder line" $T_{\rm ord}(\rho)$, denoting the onset of short-ranged A-B ordering in the fluid phase (DF, fluid without short-range order; OF, fluid with short-ranged order), is also shown by squares (MC simulation) and a solid line (PY theory). (b) Snapshot picture after 100 000 MCS/particle for $\rho^* = 0.3$ and $T^* = 0.32$ showing gas-liquid co-existence. (c) Snapshot picture after 100 000 MCS/particle for $\rho^* = 0.5$ and $T^* = 0.22$ showing gas-ordered–square-solid coexistence. Note that the two different atomic species in (b) and (c) are distinguished by dots and circles.

II C, respectively. In Sec. II D we give a short account of liquid-state integral equation theories which were used to obtain theoretical estimates for the pair distribution functions, the compressibilities, and the "disorder line" for comparison with simulation results. We discuss our results for the homogeneous fluid and the disorder line in Sec. III A and the phase diagram in Sec. III B. Finally, we conclude this paper in Sec. IV and point out possible directions of future work.

II. MODEL AND METHODS

A. The binary mixture

In order to motivate our model for the binary fluid and the particular ensemble we are interested in simulating we first recall briefly the, by now, standard model used to simulate ordering phenomena in crystalline solid mixtures. To this end, consider a perfect lattice having sites which may be occupied by an A- or B-type atom. Using occupation variables c_i^A and c_i^B ($c_i^A = 1$, if site i is occupied by a particle of type A and $c_i^A + c_i^B = 1$) one may theoretically describe such a system with Hamiltonians of the form (for a review see Ref. [1])

$$\tilde{H} = H_0 + \sum_{i<j} [c_i^A c_j^A v_{AA}(\mathbf{r}_i - \mathbf{r}_j) + 2\, c_i^A c_j^B v_{AB}(\mathbf{r}_i - \mathbf{r}_j) + c_i^B c_j^B v_{BB}(\mathbf{r}_i - \mathbf{r}_j)] + \sum_i [c_i^A \mu_A(\mathbf{r}_i) + c_i^B \mu_B(\mathbf{r}_i)]; \quad (1)$$

$\mathbf{r}_i$ is the coordinate of site i, the v's are pair potentials, μ_A and μ_B are chemical potentials, H_0 represents other degrees of freedom such as lattice vibrations, and we have

left out the trivial kinetic energy contribution. For convenience one can transform to pseudospin Ising variables $\{S_i = \pm 1\}$ using

$$c_i^A = (1 + S_i)/2, \quad c_i^B = (1 - S_i)/2 \ . \tag{2}$$

Keeping only pairwise interactions v_{AA}, v_{BB}, and v_{AB}, and neglecting any multiparticle forces for simplicity we arrive at the Ising Hamiltonian $H_{\rm Ising}$:

$$H_{\rm Ising} = -\sum_{i<j} J(\mathbf{r}_i - \mathbf{r}_j) S_i S_j - H_1 \sum_i S_i \ . \tag{3}$$

The interaction potential $J(\mathbf{r}_i - \mathbf{r}_j)$ is given by

$$J(\mathbf{r}_i - \mathbf{r}_j) = v_{AB}(\mathbf{r}_i - \mathbf{r}_j)/2 - \{v_{AA}(\mathbf{r}_i - \mathbf{r}_j) + v_{BB}(\mathbf{r}_i - \mathbf{r}_j)\}/4 \tag{4}$$

and the constant "magnetic field" H_1 contains the chemical potentials

$$H_1 = \frac{1}{2}\left\{\sum_{i \neq j} v_{AA}(\mathbf{r}_i - \mathbf{r}_j) - v_{BB}(\mathbf{r}_i - \mathbf{r}_j) - (\mu_B - \mu_A)\right\}. \tag{5}$$

Note that in this formulation one has made a change of ensemble where one goes from a grand-canonical ensemble (1) with fixed chemical potentials for both the species to a semi-grand-canonical ensemble [Eq. (3)] where only the chemical potential *difference* is fixed.

Inspired by the above formulation of the alloy Hamiltonian for a lattice system, we now introduce our simplified model designed to study an anticlustering *fluid* mixture. First, we specialize to the simple (most symmetric) case where $v_{AA} = v_{BB}$ and $\mu_A = \mu_B$ getting $H_1 = 0$ and $J(\mathbf{r}_i - \mathbf{r}_j) = \{v_{AB}(\mathbf{r}_i - \mathbf{r}_j) - v_{AA}(\mathbf{r}_i - \mathbf{r}_j)\}/2$. Second, we choose the following, square well, forms for $v_{AB}(\mathbf{r}_i - \mathbf{r}_j)$ and $v_{AA}(\mathbf{r}_i - \mathbf{r}_j)$:

$$v_{AB}(\mathbf{r}_i - \mathbf{r}_j) = \begin{cases} -\epsilon \ , & |\mathbf{r}_i - \mathbf{r}_j| < \Delta \\ 0 \ , & |\mathbf{r}_i - \mathbf{r}_j| > \Delta \ ; \end{cases} \tag{6}$$

$$v_{AA}(\mathbf{r}_i - \mathbf{r}_j) = \begin{cases} \epsilon \ , & |\mathbf{r}_i - \mathbf{r}_j| < \Delta \\ 0 \ , & |\mathbf{r}_i - \mathbf{r}_j| > \Delta \ . \end{cases} \tag{7}$$

Finally, but most importantly, we relax the constraint that the position vectors $\mathbf{r}_i$ lie on a perfect lattice and include a core-core repulsion term in the Hamiltonian to prevent the system from collapsing in the thermodynamic limit. Our (two-dimensional) model Hamiltonian therefore reads

$$H = -\sum_{i<j} J(\mathbf{r}_i - \mathbf{r}_j) S_i S_j + \sum_{i<j} U(\mathbf{r}_i - \mathbf{r}_j) \tag{8}$$

with the simple choice for the interaction potentials

$$U(r) = \begin{cases} \infty \ , & r < \sigma \\ 0 \ , & r > \sigma \ ; \end{cases} \tag{9}$$

$$J(r) = \begin{cases} -\epsilon \ , & \sigma < r < \Delta \\ 0 \ , & r > \sigma \end{cases} \tag{10}$$

for the interaction potentials. We complete the definition of the Hamiltonian by choosing the nontrivial value (see Sec. III) $\Delta = 1.4\sigma$ for the width parameter and $\epsilon = 1$ to fix the arbitrary energy scale.

Our model system thus consists of disks in two dimensions which have an additional Ising spin degree of freedom attached and the interaction between the disks consists of a hard disk part and a square well (step) part if the spins point in opposite (same) directions. These Ising spins are allowed to flip, thus enabling one to change the identity of any particular disk. This additional degree of freedom (present in the chosen semi-grand-canonical ensemble) is expected to improve the equilibration *dynamics* of the model though the values of the various thermodynamic quantities in the thermodynamic limit should be the same as that obtained by keeping the spins fixed in time (as one would do in the standard canonical ensemble), a fact which was explicitly checked by us.

B. Details of the simulations

We perform Monte Carlo simulations [12,2] for the system described by Hamiltonian (8) with $N = 1000$ particles in a two-dimensional square box of area (volume) V with periodic boundary conditions. We use the well known Metropolis algorithm to make particle displacements and spin moves starting from either a configuration generated by a previous run or from a high temperature configuration with random particle positions and randomized spins with total magnetization $M = \sum_i S_i = 0$. Typically at any state point, we simulate for about 10–20 000 Monte Carlo steps (MCS)/particle in order to ensure that equilibrium is achieved; the various averages are then calculated over a further 100 000 MCS/particle. During the course of the simulation the fraction of up and down spins fluctuate around 1/2. This is only to be expected since our system is symmetric with respect to A and B particles so that a state corresponding to equal chemical potentials results in equal molar fractions of A and B atoms.

The density $\rho^\star = \rho\sigma^2 = (N/V)\sigma^2$ of the system is varied between 0 and 0.7 and the temperature $T^\star = \beta^{-1}/k_B\epsilon$ between 0.2 and 1.3, such that typical fluid parameters were set up, except at densities above 0.65 and temperatures below 0.3, where (square lattice) solid structures are found (see Sec. III B). We calculate the partial pair distribution functions $g_{\nu\mu}(r)$, the average energy, the specific heat, and the density distribution function $P_L(\rho)$ (see Sec. II C), from which fluid state isothermal compressibilities $\rho k_B T \chi_T(\rho, T)$ and the coexistence densities $\rho_{\rm gas}$, $\rho_{\rm liq}$, and $\rho_{\rm solid}$ in the two-phase regions were obtained in the thermodynamic limit (see Sec. II C).

C. The block analysis technique

In this subsection we give a brief account of the block analysis technique which has been used to obtain fluid

state compressibilities and the gas-liquid and gas-solid coexistence curve for our model in the thermodynamic limit. By now, this is a rather well known and reliable method that has been used to obtain useful information in lattice systems [13], classical fluids [14], and recently in a "quantum spin fluid" [9]. This method is an extension of finite size scaling techniques which are a standard tool for the analysis of phase transitions of *lattice* models [2,12].

The key idea consists of dividing the system into a number of subsystems, of length L, and building up the density distribution function $P_L(\rho)$ by keeping track of the density fluctuations in these subsystems; the density of the total system is, of course, strictly constant in our Monte Carlo simulation in the NVT ensemble. The densities of coexisting phases can be estimated reliably from the distribution function. The behavior of the compressibility [14,9] and the location of the critical point [14,9] can also be extracted from the information contained in the distribution functions. Before going into more detail, a few words with respect to the Gibbs-ensemble method [15] are in order. While the spirit of the Gibbs–ensemble approach is related to the attractive idea of *directly* studying phase coexistence between two system cells, one cell being in the fluid state and one in the gas state, which can exchange atoms at constant pressure [15], the distinguishing feature of our approach is the possibility to systematically studying size effects on relevant quantities. As will be demonstrated explicitly in Sec. III we find such extrapolations to the thermodynamic limit *crucial* in the case under consideration; first investigations of size effects in a restricted version of the Gibbs-ensemble are presented in Ref. [16]. Also the Gibbs-ensemble method in practice works only for fluid-state (gas-liquid and fluid-fluid) phase equilibria, while the present technique, although it may need more computational effort, is straightforwardly useful to identify solid phases as well [cf. Figs. 1(a) and 1(c)].

In the statistical mechanics of many body systems it is a familiar concept [17] to divide the system into *cells* or *blocks* of finite dimension L. Defining the particle number in the block as N_i, with $\sum_i N_i = N$, the density ρ_i in the ith block becomes

$$\rho_i = \frac{N_i}{L^d}, \quad L = \frac{S}{M_b}, \tag{11}$$

where M_b is an integer and S is the linear dimension of the total system ($V = S^d$ in d dimensions). Thus $(S/L)^d = M_b^d$ subsystems are studied simultaneously which improves the statistics. Note also that in one simulation run we use the same particle configurations to investigate several choices of M_b simultaneously, and thus the study of a single (but large enough) system already allows an estimation of finite size effects.

We focus attention on the moments of the distribution function

$$\langle \rho^k \rangle_L = \int \rho^k P_L(\rho) d\rho \ , \tag{12}$$

where $P_L(\rho)$ is the average of the density distributions $P_L(\rho_i)$ for $i = 1, \ldots, M_b^d$, i.e., all subsystems are averaged together. The zeroth moment is fixed by normalization of probabilities and the first moment is of no interest either, since $\langle \rho \rangle = N/S^d$ is held fixed. The second moment, by standard fluctuation relations [17], is related to the isothermal compressibility

$$\begin{aligned} \langle (\Delta\rho)^2 \rangle_L &= \langle (\rho - \langle \rho \rangle)^2 \rangle_L \\ &= L^{-d} \langle \rho \rangle^2 k_B T \chi_T^{(L)} \ ; \end{aligned} \tag{13}$$

here our notation emphasizes that $\chi_T^{(L)}$ is the standard isothermal compressibility only in the thermodynamic limit $N \to \infty$ and hence $L \to \infty$, while for small L we expect systematic deviations due to finite size effects. For a state within the one-phase region, the distribution $P_L(\rho)$ is approximately Gaussian if L by far exceeds the correlation length ξ of the order parameter fluctuations (i.e., density fluctuations), $L \gg \xi$,

$$\begin{aligned} P_L(\rho) &= \frac{L^{d/2}}{(2\pi \langle (\Delta\rho)^2 \rangle_L)^{1/2}} \exp\left[-\frac{(\Delta\rho)^2}{2\langle (\Delta\rho)^2 \rangle_L} \right] \\ &\propto \exp\left[-\frac{(\Delta\rho)^2 L^d}{2\langle \rho \rangle^2 k_B T \chi_T^{(L)}} \right] . \end{aligned} \tag{14}$$

This relation suggests that one can extract the system compressibility in the one-phase region by fitting Gaussian functions to the average density distribution functions $P_L(\rho)$. Assuming a leading boundary correction term χ_T^{BC} the fitted (L-dependent) compressibilities $\chi_T^{(L)}$ can then be plotted against $1/L$ or M_b

$$\chi_T^{(L)} = \chi_T \left[1 - \chi_T^{\mathrm{BC}} \left(\frac{\xi}{L} \right) \right] \tag{15}$$

and $\chi_T \equiv \chi_T^{(\infty)}$ can be extracted by extrapolating to $M_b = 0$.

The situation is different for a state in a two-phase region where (14) has to be replaced by a combination of two Gaussian functions

$$\begin{aligned} P_L(\rho) \propto & \frac{\rho_{\mathrm{liq}}^{(L)} - \langle \rho \rangle}{\rho_{\mathrm{liq}}^{(L)} - \rho_{\mathrm{gas}}^{(L)}} \frac{1}{\rho_{\mathrm{gas}}^{(L)} \sqrt{\chi_T^{\mathrm{gas}}}} \exp\left[\frac{-(\rho - \rho_{\mathrm{gas}}^{(L)})^2 L^d}{2(\rho_{\mathrm{gas}}^{(L)})^2 k_B T \chi_T^{\mathrm{gas}}} \right] \\ & + \frac{\langle \rho \rangle - \rho_{\mathrm{gas}}^{(L)}}{\rho_{\mathrm{liq}}^{(L)} - \rho_{\mathrm{gas}}^{(L)}} \frac{1}{\rho_{\mathrm{liq}}^{(L)} \sqrt{\chi_T^{\mathrm{liq}}}} \\ & \times \exp\left[\frac{-(\rho - \rho_{\mathrm{liq}}^{(L)})^2 L^d}{2(\rho_{\mathrm{liq}}^{(L)})^2 k_B T \chi_T^{\mathrm{liq}}} \right] , \end{aligned} \tag{16}$$

again assuming that $L \gg \xi$; for notational simplicity we specialize here to gas-liquid coexistence and only mention that an analogous formula applies for gas-solid coexistence. The relative weights of the two phases are fixed according to the *lever rule* [17,14].

In the ansatz (16) we have approximated the distribution function as a superposition of two Gaussian functions centered around the densities $\rho_{\mathrm{gas}}^{(L)}$ and $\rho_{\mathrm{liq}}^{(L)}$ of the two coexisting phases. Thus (16) is *not exact* even in the

limit $L \gg \xi$, since interfacial free energy contributions are neglected [13,14,9]. It can be shown in analogy to the arguments presented for lattice gas model that, for $\rho_{\rm gas} < \rho < \rho_{\rm liq}$, the decrease of $\ln P_L(\rho)$ is not proportional to the volume, as suggested by (16),

$$\ln P_L(\rho) \propto -L^d, \tag{17}$$

but the leading decay occurs proportionally to the interface area

$$\ln P_L(\rho) \propto -L^{d-1}\,. \tag{18}$$

Nevertheless we stress and we will demonstrate in the result section that (16) is a useful concept to describe the system for densities ρ in the vicinity of the gas or liquid density. Similarly one can obtain the coexistence densities in the thermodynamic limit

$$\rho_{\rm coex}^{(L)} = \rho_{\rm coex}\left[1 - \rho_{\rm coex}^{\rm BC}\left(\frac{\xi}{L}\right)\right]\,, \tag{19}$$

assuming a leading interface correction term $\rho_{\rm coex}^{\rm BC}$.

To obtain the phase diagram one places simulation points in the two-phase region and obtains the distribution functions $P_L(\rho)$. The position of the peaks in the distribution functions may then be used to obtain (L-dependent) coexistence densities. In general an extrapolation $L \to \infty$ (19) is then required to obtain the phase diagram in the *thermodynamic limit*. While it is true that for average densities well within the spinodal region one expects to see a double peaked form for $P_L(\rho)$ as suggested by (16) we point out here that very long simulation times may be required to allow for the system to coarsen sufficiently such that this is actually observed. We have found that the phase diagram may be mapped most efficiently by placing simulation points close to the expected liquid and gas coexistence densities based on extrapolation of the coexistence curve calculated from previous runs.

D. Integral equation theories for fluid-state distribution functions

We have computed fluid state partial pair distribution functions and the compressibility from standard liquid-state theories to compare with our simulation results. We include here a short discussion introducing these integral equation theories for liquid mixtures mainly for completeness; detailed information can be obtained from such standard texts as Ref. [18].

For an isotropic, homogeneous fluid mixture of p components with composition x_μ ($\mu = 1, \ldots, p$) the Ornstein-Zernike equation [18] relating the pair correlation function $h_{\mu\nu}(r) = g_{\mu\nu}(r) - 1$ to the direct correlation function $c_{\mu\nu}(r)$ takes the form

$$h_{\nu\mu}(r) = c_{\nu\mu}(r) + \rho \sum_\lambda x_\lambda \int c_{\nu\lambda}(|\mathbf{r} - \mathbf{r}'|)\; h_{\lambda\mu}(r')\; d\mathbf{r}'\,. \tag{20}$$

The above equation states that the total correlation in a fluid between two particles of species μ and ν consists of a direct part denoted by $c_{\mu\nu}(r)$ and an indirect part mediated by all other particles in the system. Equation (20) can be taken to be a definition for the direct correlation function. To obtain the partial pair distribution functions we need another equation (a closure condition) which involves $c_{\mu\nu}(r)$ and $h_{\mu\nu}(r)$. Various approximate closure conditions exists in the literature [18] which may be used to obtain reliable estimates for the distribution functions, but the accuracy of any one of these approximations is difficult to predict *a priori*. We have checked our simulation results against the predictions of three different closure approximations: the hypernetted chain (HNC), the Percus-Yevick (PY), and the mean spherical approximation (MSA) given by

$$g_{\nu\mu}(r) = \begin{cases} \exp\{-\beta V_{\nu\mu}(r)\}\exp\{h_{\nu\mu}(r) - c_{\nu\mu}(r)\} & \text{(HNC)} \\ \exp\{-\beta V_{\nu\mu}(r)\}\{1 + h_{\nu\mu}(r) - c_{\nu\mu}(r)\} & \text{(PY)} \\ \exp\{-\beta V_{\nu\mu}^0(r)\}\{1 + h_{\nu\mu}(r) - c_{\nu\mu}(r) - \beta V_{\nu\mu}^1(r)\} & \text{(MSA)}\,. \end{cases} \tag{21}$$

The pair potential between species μ and ν has been denoted by $V_{\mu\nu}(r)$. Note that for the MSA closure one needs to separate the interaction into a purely repulsive hard core $V_{\nu\mu}^{(0)}$ and a tail $V_{\nu\mu}^{(1)}$ whose nature depends on the species involved, i.e., attractive for AB and repulsive for AA or BB in our model. We solve these equations numerically using the efficient algorithm of Gillan [19] in two dimensions for various densities and temperatures for the composition $x_A = x_B = 1/2$. Our results are discussed in Sec. III A.

Once the partial distribution functions are obtained, it is a simple matter to compute the isothermal compressibility χ_T for the binary mixture

$$\sum_{\nu\mu} x_\nu x_\mu \rho \tilde{c}_{\nu\mu}(0) = 1 - \chi_T^0/\chi_T \tag{22}$$

with $\rho k_B T \chi_T^0 = 1$; $\tilde{c}$ denotes the Fourier transform of c.

III. RESULTS AND DISCUSSION

A. The homogeneous fluid

In Fig. 2 we compare the results for the pair distribution functions $g_{\nu\mu} = h_{\nu\mu} + 1$ obtained from the simulation with the results of the integral equation theories for $\rho^\star = 0.5$ and $T^\star = 1.0$. In this region of the phase diagram we find excellent agreement with the Percus-Yevick result, whereas the hypernetted chain and the mean spherical approximations are seen to be considerably poorer. Note the density enhancement of B particles around A particles and short-ranged concentration fluctuations reminiscent of ionic liquids [20]. To compare further our simulation results with the prediction of liquid state integral equation theories, we focus on the isothermal compressibility χ_T. In the fluid phase the density distribution in subsystems of size $\xi \ll L \ll S$ is found

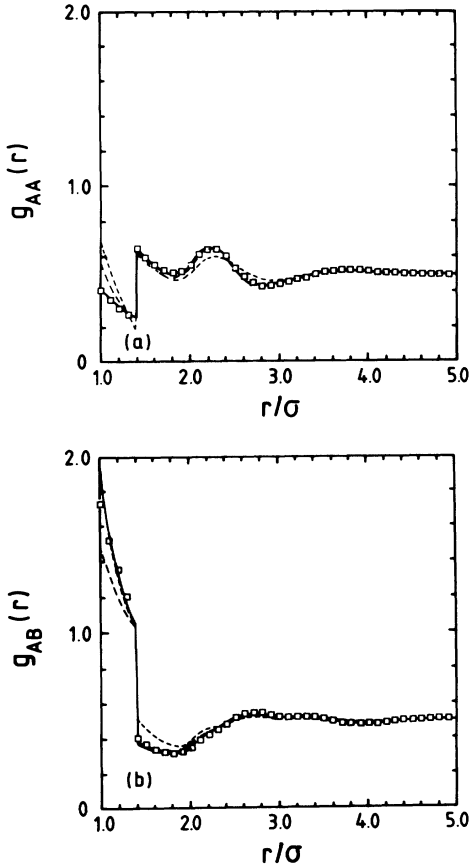

FIG. 2. Pair distribution functions (a) $g_{AA}(r)$ and (b) $g_{AB}(r)$ in the fluid phase ($T^* = 1$, $\rho^* = 0.5$). Simulation data (symbols) and results from various integral equation theories (lines) as described in the text. Solid line, PY; long dashed line, HNC; short dashed line, MSA.

to be a Gaussian function as explicitly demonstrated by showing the fits using (14) with variable prefactor and width; see Fig. 3(a). The subsystem size dependent compressibilities $\chi_T^{(L)}$ can be obtained from the fitted widths using (13). In Fig. 3(b) we show a scaling plot (15) of the compressibilities $\chi_T^{(L)}$ to the thermodynamic limit χ_T by extrapolating $M_b \to 0$. We note an *excellent* agreement of this value with the result of the Percus-Yevick theory marked with a cross at $M_b = 0$; using only the largest (useful) subsystem without extrapolation would yield a value being 10% too high. We remind the reader that it is not at all straightforward to obtain such compressibilities in the *thermodynamic limit* using grand-canonical or Gibbs-ensemble methods. However, such good agreement is only possible at high temperatures, far away from the critical point. Upon lowering the temperature we observe first of all a dramatic increase of χ_T especially for $\rho^* = 0.3$, which already signals the critical point of the gas-liquid coexistence region. Investing considerably more computer time (to determine accurately the critical point and then approaching it close enough to measure χ_T) we could in principle even obtain the corresponding critical exponent. In addition to this we observe large differences between the Monte Carlo values of the com-

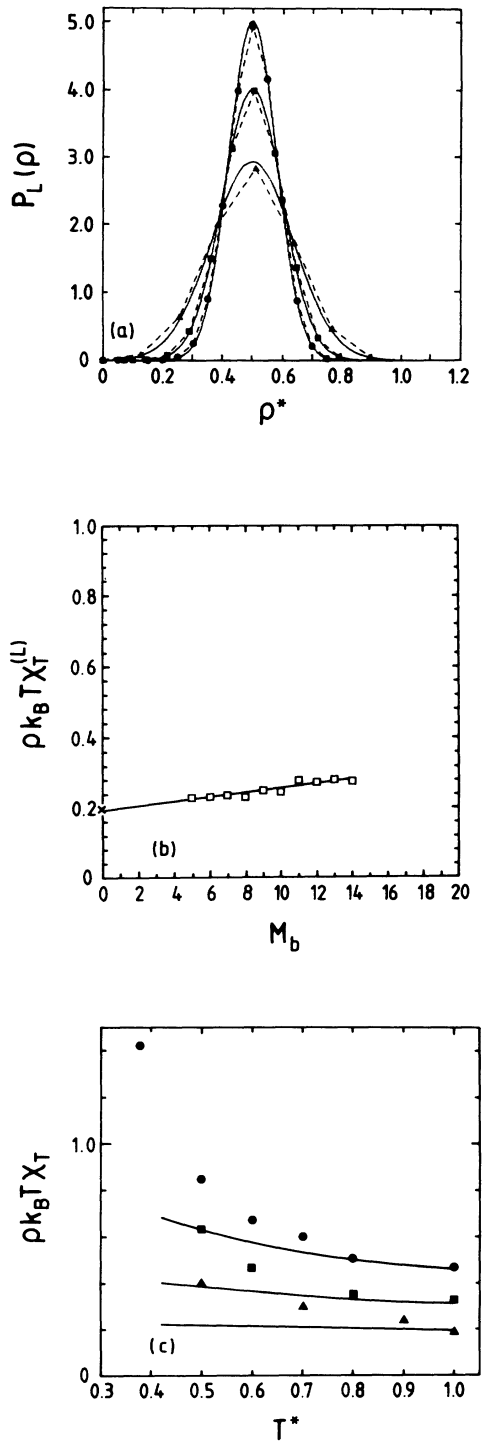

FIG. 3. (a) Density distributions $P_L(\rho)$ for various blockings $M_b = 10$ (circles), 12 (squares), and 16 (triangles), and the corresponding Gaussian fits (full lines) in the fluid phase ($T^* = 1$, $\rho^* = 0.5$). (b) Comparison of simulation and PY values for the isothermal compressibility at $\rho^* = 0.5$, $T^* = 1$. The cross denotes the PY value $\rho k_B T \chi_T$, the squares denote the simulation results $\rho k_B T \chi_T^{(L)}$ in different subsystems of size M_b, and the line is a linear fit of the simulation data. (c) Plot of the isothermal compressibility in the thermodynamic limit $\rho k_B T \chi_T$ versus T^* for densities $\rho^* = 0.3$ (circles), 0.4 (squares), and 0.5 (triangles). The lines denote corresponding PY results and agree at high temperatures with the simulation data.

pressibilities and the Percus-Yevick results, see Fig. 3(c), even at temperatures twice as large as the critical temperature where we believe the simple extrapolation relying on (15) to be still valid. These deviations are due to the diverging correlation length and consequently a breakdown of the Percus-Yevick approximation. Although it may be possible to devise better integral equation theories [21] which are expected to be valid also near the critical point, we do not embark on such an endeavor here.

Next, we attempt to quantify the short-ranged A-B ordering in the *fluid* state in the following way. We begin by defining a function $F(r)$

$$F(r) = \frac{g_{AA}(r) - g_{AB}(r)}{g_{AA}(r) + g_{AB}(r)} \tag{23}$$

guided by the idea that this quantity is an r-dependent measure of the difference in the concentration of the species.

The asymptotic decay of $F(r)$ may be either uniformly positive ($F(r) \propto \exp[-r/\xi]$) or oscillatory ($F(r) \propto \exp[-r/\xi]\cos(\alpha r + \phi)$), where α characterizes the period of oscillations. If in the parameter space of the model a line exists which separates these two behaviors, one calls this line disorder line [23]. In the context of simulations, however, it is more convenient to consider a related behavior of the Fourier transform: In the case of no order the Fourier transform $\tilde{F}(q)$ is expected to show only a trivial maximum at $q = 0$, whereas a maximum at nonvanishing q values can only occur if some kind of short-range order on a length scale $\sim q^{-1}$ is present in the liquid. In Fig. 4(a) we present this function $\tilde{F}(q)$ for one density and different temperatures and one can clearly distinguish two regimes with and without a maximum at $q_{\max} \neq 0$. Thus, below a density-dependent "transition temperature" we find some kind on short-ranged order in the fluid. The type of this ordering is visualized in the configuration snapshot in Fig. 1(b): the liquid patches possess *locally* an ordering of the type $\cdots$-A-B-A-B-$\cdots$ along mildly curved lines which is reminiscent from the perfect unfrustrated antiferromagnetic A-B ordering of the square lattice solid in Fig. 1(c). While this is not a phase transition (the specific heat and the compressibility show no singularities) it represents a sharp change in the nature of *short-range* order in the fluid. This maximum wave number $q_{\max} \neq 0$ is plotted for different densities versus temperature in Fig. 4(b) and we can locate the corresponding effective transition temperature $T_{\rm ord}$ by the sharp jump of $q_{\max}$. The resulting short-range "disorder line" $T_{\rm ord}(\rho)$ is presented in the phase diagram Fig. 1(a) (squares) as a function of the density. Having integral equation solutions for the radial distribution functions we can also calculate this curve using this approach. We have used the best approximation for the present $g_{\nu\mu}(r)$, the Percus-Yevick closure, to obtain a theoretical estimate for $T_{\rm ord}(\rho)$, which is also shown in the same figure as a line. Although the theoretical curve is qualitatively similar and even quantitatively correct at high temperatures, we note deviations from the simulation results mainly at low temperatures since the Percus-Yevick approximation for $g(r)$ becomes worse. Related curves where the behavior of correlation functions change (disorder lines) have occasionally been discussed for various lattice models [23], but to our knowledge this is the first time that such a line has been found for an *off-lattice* continuum model of a fluid.

B. The phase diagram

We have used the block analysis technique described in Sec. II C to obtain the phase diagram shown in Fig. 1(a). Below a critical temperature $T_c \approx 0.37$ we observe a flat two-phase region with coexisting gas and liquid phases. The usefulness of the block analysis method in conjunction with the Gaussian approximation even for such difficult problems is self-evident. The coexistence densities were obtained by placing simulation points close to the "expected" phase boundaries (based on extrapolation of data obtained from previous runs) inside the coexistence region, and extracting the peak positions of the density distribution functions; see Figs. 5(a), 5(c),

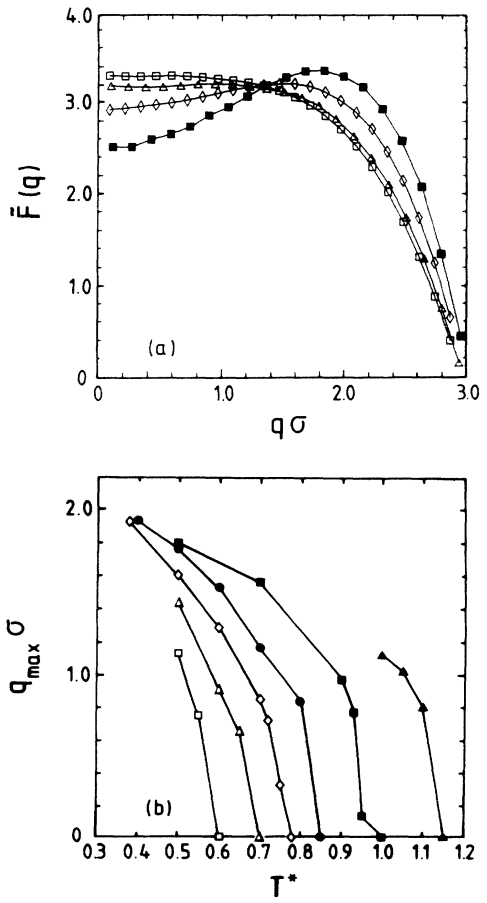

FIG. 4. (a) Function $\tilde{F}(q)$ (defined in the text) versus q for different temperatures at $\rho^* = 0.5$. At $T^* < 0.9$ we observe the onset of a maximum of $\tilde{F}(q)$ at a nonzero value of q. Symbols show simulation results for $T^* = 1$ (open squares), 0.9 (triangles), 0.7 (diamonds), and 0.5 (filled squares). (b) Position of the $q \neq 0$ maximum of $\tilde{F}(q)$ versus T^* for $\rho^* = 0.1$ (open squares), 0.2 (open triangles), 0.3 (diamonds), 0.4 (filled circles), 0.5 (filled squares), and 0.6 (filled triangles). The points are joined by lines for visual help.

and 5(e) for typical samples from the gas, liquid, and solid regimes. Contrary to our previous experience with the block analysis [14,9] a finite size scaling also of the coexistence densities was *crucial* to obtain meaningful results especially in the gas phase. Thus the position of the peaks in these distribution functions $\rho_{\text{coex}}^{(L)}$ were plotted as a function of M_b as suggested by (19) and the values for the coexistence densities in the thermodynamic limit ρ_{coex} were obtained from extrapolation to $M_b = 0$; see Figs. 5(b) and 5(d). The observed size dependence in the gas phase is dramatic, see Fig. 5(b), whereas the solid phase does not show any size effects within the statistical scatter of the distributions, see Fig. 5(e), and the liquid phase densities are subject to only mild shifts, see Fig. 5(d).

The strong size effects on the density distribution can be qualitatively rationalized by inspecting representative configurations. We show typical snapshot pictures after about 100 000 MCS/particle in the gas-liquid [Fig. 1(b)] and in the gas-solid regions [Fig. 1(c)]. The gas-liquid interface appears to be unusually "rough" although the system has been quenched deep in the two-phase region ($\rho^\star = 0.3$, $T^\star = 0.32$). The coarsening dynamics is also seen to be extremely slow and a double peaked structure [9] for $P_L(\rho)$ was never observed by us at any length scale L for this system within our simulation times. The gas phase seems for our systems size of 1000 particles not well separated from the liquid phase as in usual cases, but it is rather formed by filamentlike or meander-like structures near liquid droplets. At some places one can even recognize quasi-one-dimensional structures of liq-*A*-*B*-*A*-*B*-$\cdots$ strings anchored with one end at a liquid droplet.

The solid phase is well defined and possesses at sufficiently low densities an *A*-*B* ordered square lattice structure; see Fig. 1(c). This phase is stabilized since it allows for a complete *unfrustrated* $\cdots$-*A*-*B*-*A*-*B*-$\cdots$ antiferromagnetic ordering in two (orthogonal) directions in two dimensions. Note that this is different from the mechanism in a similar ferromagnetic model in Ref. [9] where a width parameter of $\Delta' = 1.5\sigma$ stabilizes [9] the square lattice at some region in the phase diagram: in case of a square lattice the four nearest and four next-nearest neighbors can lower the magnetic energy by 8ϵ, whereas the six nearest neighbors of the triangular lattice can only contribute by 6ϵ. In the present case with an antiferromagnetic interaction the basic plaquette (and the complete infinite system) of the square lattice is unfrustrated with respect to *A*-*B* substitutional order, whereas the corresponding triangular plaquette has to be frustrated. As the system is compressed we expect a transition to a hexagonal phase which is the close packing limit for hard disks; however, the *A*-*B* ordering in this triangular phase is necessarily frustrated.

Finally we mention that even with the large density difference between liquid and solid, see Fig. 1(a), we cannot use the density block analysis method for mapping that part of the phase diagram, but rather a method as devised in Ref. [11] would be appropriate. On the other hand, we can obtain reliably the gas-solid coexistence densities from the block analysis. The distribution function $P_L(\rho)$ for the same statepoint ($\rho^\star = 0.5$, $T^\star = 0.22$) as the snapshot Fig. 1(c) is shown in Fig. 5(c). The prominent square solid regions result in well defined peaks on many length scales, whereas the density of the gas phase is so small that it cannot be resolved any more with the given particle number so that a zero density peak appears in the density distribution. The fact that the surfaces of the solid are smooth, see Fig. 1(c), is reflected in the density plot Fig. 5(c): the peak positions corresponding to $\rho_{\text{sol}}^{(L)}$ do not show any systematic size dependence for the given resolution. Another quantity which we can reliably estimate from the block analysis is the triple temperature $T_{\text{triple}}^\star = 0.3$ from the associated sharp density jump in the phase diagram; see Fig. 1(a). Furthermore the solid coexistence density does not increase as the temperature is lowered considerably below the triple temperature.

Another possibly interesting observation is the presence of pronounced four-fold local order in the *liquid* phase (the fluid phase was already discussed in Sec. III A) similar to the solid phase; compare Fig. 1(c) with the liquid regions in Fig. 1(b). This may indicate the possible presence of a tetratic phase [22] as discussed in the framework of two-dimensional melting [22]. However, our present tools (the block density distributions and the pair distribution functions) are, of course, not designed to probe such *angular ordering* phenomena; extensive developments and investigations aiming to implement block distributions for bond-orientational order parameters [25,11] are currently in progress [24].

IV. SUMMARY, CONCLUSIONS, AND FUTURE DIRECTIONS

In summary, we have introduced a model system in two dimensions which is designed to study the competition between ordering and packing tendencies expected to be present in *liquid* anticlustering binary alloys. Two techniques were used in this investigation: Monte Carlo simulations in conjunction with finite size scaling in form of the block analysis technique for density distributions and analytical liquid state theories. Deep in the fluid phase we find excellent agreement with the integral equation theories for the radial distribution functions and compressibilites; the latter could be obtained from the simulations in the thermodynamic limit. When approaching the critical point the analytical results start to deviate considerably from the simulation data.

The major goal of the study was the detailed mapping of the low-temperature–low-density part of the phase diagram. We find the fluid phase to be *locally* structured with respect to *A*-*B* ordering below a "disorder line" which can also be obtained analytically in the high-temperature regime. Although frustration of the ordering tendency leads to no long-ranged order in the fluid state, the lowering of the free energy produced by *short-ranged* *A*-*B* order in the liquid is sufficient to produce a liquid-gas transition in this system. The low-temperature solid phase has a long-ranged *A*-*B* ordered square lattice structure for sufficiently low densities. At high temperatures

one expects the solid phase to have a substitutionally frustrated triangular lattice with no long-ranged A-B order. However, we devoted the present study to liquid-state properties and a thorough study of this part of the phase diagram requires the use of block distribution functions using bond-orientational order parameters [25,11] which is currently under investigation [24]. The possible presence of a tetratic phase [22] having strong fourfold

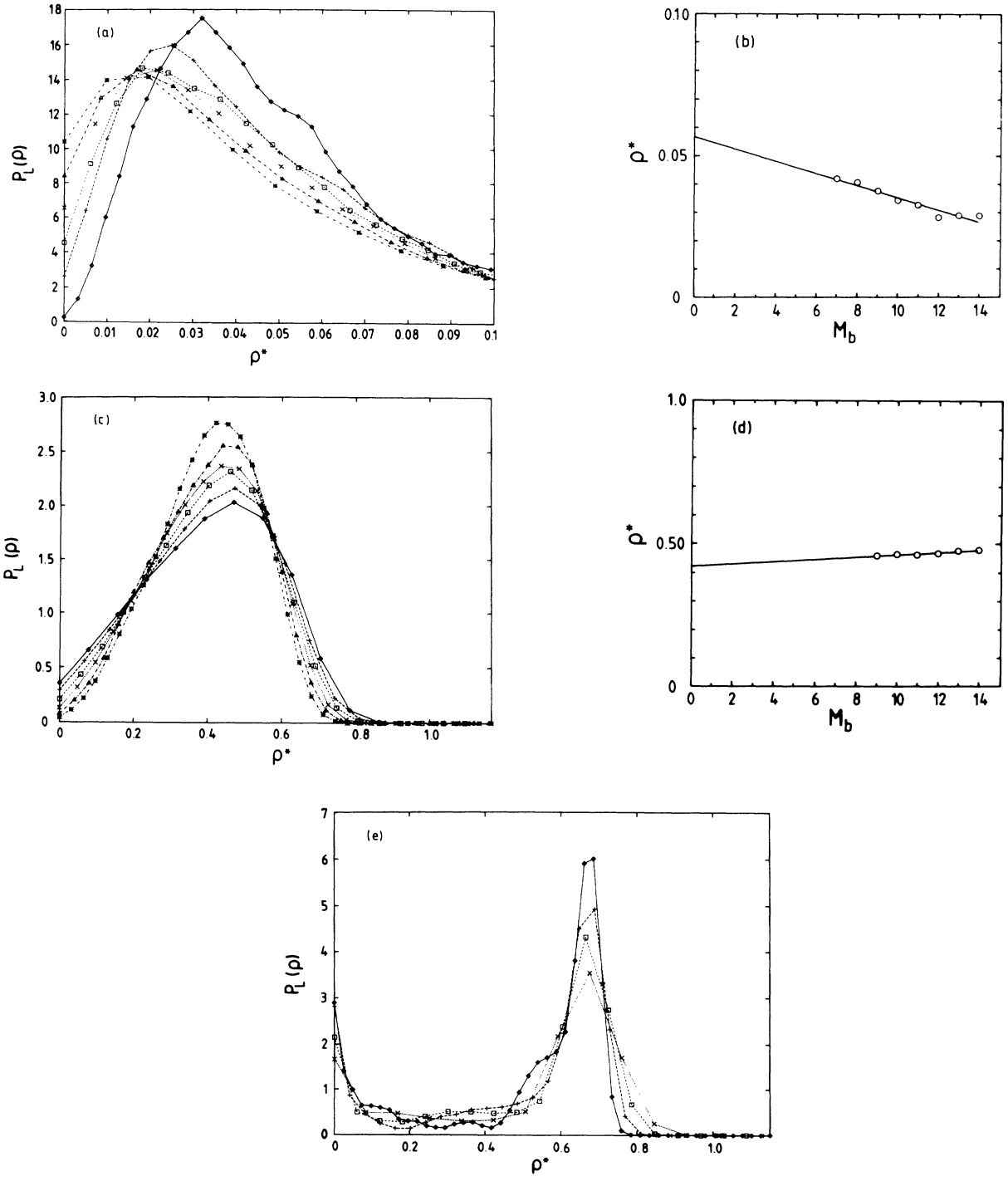

FIG. 5. Density distribution $P_L(\rho)$ in subsystems and finite size extrapolation of coexistence densities. (a) $P_L(\rho)$ versus ρ^* for a typical state point in the two phase region close to the gas phase ($\rho^* = 0.05$, $T^* = 0.26$). The density distributions are shown for $M_b = 9$–14 (larger M_b results in flatter curves). (b) Plot of the position of the peaks of $P_L(\rho)$ as a function of M_b; the infinite system limit is taken by extrapolating the linear fit to $M_b = 0$. (c) and (d) as in (a) and (b) but for ($\rho^* = 0.4$, $T^* = 0.32$). (e) $P_L(\rho)$ in the gas-solid coexistence region, for $M_b = 8, 10, 12$, and 14 ($\rho^* = 0.5$, $T^* = 0.22$); note that the peak positions are independent of the length scale and the presence of a zero density gas peak in addition to the high density peak corresponding to the solid.

bond-orientational order with no long-ranged positional order is also a challenging project for future investigations.

ACKNOWLEDGMENTS

The authors thank B. Dünweg and M. Barma for useful discussions. The support from the Deutsche Forschungsgemeinschaft for D.M. (Bi 314/5 und Forschungsstipendium) and P.N. (Heisenberg Foundation) is gratefully acknowledged. And last but not least the present study would have been impossible without grants of computer time on the Cray-YMP (HLRZ Jülich), VP 100 (RHRK Kaiserslautern), and IBM RISC System/6000 cluster (ZDV Mainz).

[1] K. Binder, in *Festkörperprobleme (Advances in Solid State Physics)*, edited by P. Grosse (Vieweg, Braunschweig, 1986), Vol. 26, p. 133; D. de Fontaine, in *Solid State Physics*, edited by H. Ehrenreich, F. Seitz, and D. Turnbull (London, Academic, 1979), Vol. 34. p. 73; W. Pitsch and G. Inden, in *Phase Transformations in Materials*, edited by P. Haasen (VCH, Weinheim, 1991), p. 497; *Alloy Phase Stability*, edited by A. Gonis and G. M. Stocks (Elsevier, New York, 1988).

[2] *Monte Carlo Methods in Statistical Physics*, edited by K. Binder (Springer, Berlin, 1979); *Applications of the Monte Carlo Methods in Statistical Physics* (Springer, Berlin, 1984); *Monte Carlo Methods in Condensed Matter Physics* (Springer, Berlin, 1992).

[3] F. Schmid and K. Binder, J. Phys. Condens. Matter **4**, 3569 (1992).

[4] K. Binder and D. P. Landau, Phys. Rev. B **21**, 1941 (1980).

[5] R. Kikuchi, Phys. Rev. **81**, 988 (1951).

[6] B. Dünweg and K. Binder, Phys. Rev. B **36**, 6935 (1987).

[7] W. G. T. Kranendonk and D. Frenkel, J. Phys. Condens. Matter **1**, 7735 (1989).

[8] *Ordering in Two Dimensions*, edited by S. K. Sinha (North-Holland, Amsterdam, 1980); *Phase Transitions in Surface Films 2*, edited by H. Taub, G. Torzo, H. J. Lauter, and S. C. Fain (Plenum, New York, 1991).

[9] D. Marx, P. Nielaba, and K. Binder, Phys. Rev. Lett. **67**, 3124 (1991); D. Marx, Surf. Sci. **272**, 198 (1992); D. Marx, P. Nielaba, and K. Binder, Phys. Rev. B **47**, 7788 (1993); D. Marx, in *Computer Simulation Studies in Condensed Matter Physics VI*, edited by D. L. Landau, K. K. Mon, and H. B. Schüttler (Springer, Berlin, 1993), p. 100.

[10] S. Sengupta, D. Marx, and P. Nielaba, Europhys. Lett. **20**, 383 (1992).

[11] A. C. Mitus, D. Marx, S. Sengupta, P. Nielaba, A. Z. Patashinskii, and H. Hahn, J. Phys.: Condens. Matter **5**, 8509 (1993).

[12] K. Binder and D. W. Heermann, *Monte Carlo Simulation in Statistical Physics—An Introduction* (Springer, Berlin, 1988).

[13] K. Binder, Z. Phys. B **43**, 119 (1981).

[14] M. Rovere, D. W. Heermann, and K. Binder, Europhys. Lett. **6**, 585 (1988); J. Phys. Condens. Matter **2**, 7009 (1990); M. Rovere, P. Nielaba, and K. Binder, Z. Phys. B **90**, 215 (1993).

[15] A. Z. Panagiatopoulos, Mol. Phys. **61**, 813 (1987); for a review see Mol. Simulation **9**, 1 (1992).

[16] K. K. Mon and K. Binder, J. Chem. Phys. **96**, 6989 (1992); K. K. Mon, Phys. Rev. B **47**, 5497 (1993).

[17] L. D. Landau and E. M. Lifshitz, *Statistical Physics* (Pergamon, London, 1980)

[18] J. P. Hansen and I. R. McDonald, *Theory of Simple Liquids* (Academic, London, 1986).

[19] M. J. Gillan, Mol. Phys. **38**, 1781 (1979).

[20] J. E. Enderby, J. Phys.: Condens. Matter **5**, B99 (1993).

[21] G. Zerah and J. P. Hansen, J. Chem. Phys. **84**, 2336 (1986).

[22] D. R. Nelson and B. I. Halperin, Phys. Rev. B **19**, 2457 (1979); A. P. Young, *ibid.* **19**, 1855 (1979); K. J. Strandburg, Rev. Mod. Phys. **60**, 161 (1988); H. Kleinert, *Gauge Fields in Condensed Matter*, (World Scientific, Singapore, 1989), Vol. II, Pt. III, Chap. 14; M. A. Glaser and N. A. Clark, Adv. Chem. Phys. (to be published).

[23] J. Stephenson, Can. J. Phys. **48**, 1724 (1990); R. Liebmann, in *Statistical Mechanics of Periodic Frustrated Ising Systems*, edited by H. Araki, J. Ehlers, K. Hepp, R. Kippenhahn, H. A. Weidenmüller, and J. Zittartz, Lecture Notes in Physics Vol. 251 (Springer, Berlin, 1986); R. M. Hornreich, R. Leibmann, H. G. Schuster, and W. Selke, Z. Phys. B **35**, 91 (1979); W. Selke, Phys. Rep. **170**, 213 (1988).

[24] H. Weber, D. Marx, and K. Binder (unpublished).

[25] D. R. Nelson and J. Toner, Phys. Rev. B **24**, 363 (1981); P. J. Steinhardt, D. R. Nelson, and M. Ronchetti, *ibid.* **28**, 784 (1983).